CHAPTER II
LITERATURE REVIEW

2.1 Hydrogen: Fuel of the Future

Hydrogen is now being considered as an ideal fuel for the future. Hydrogen fuel can be produced from clean and renewable energy sources, and thus, its life cycle is clean and renewable. Solar and wind are the two major sources of renewable energy, and they are also the promising sources for renewable hydrogen production. However, presently, renewable energy contributes only about 5 % of the commercial hydrogen production primarily via water electrolysis, while other 95 % hydrogen is mainly derived from fossil fuels (Bak *et al.*, 2002). Hydrogen is a carrier of energy, not a source. It does not exist in a natural state on earth and must be manufactured using a hydrogen-rich compound as the raw material. Moreover, hydrogen can be used for the powering of non-polluting vehicles, domestic heating, and aircraft. Today, hydrogen is produced mainly through steam reforming of natural gas, but it can be extracted from other hydrocarbons by reforming or partial oxidation. A major shortcoming of the processing of hydrocarbons is the resulting emissions of carbon and airborne pollutants. Most of other production processes in use or under development involve the electrolysis of water by electricity. This method produces no emissions, but is typically more costly compared to hydrocarbon reforming or oxidation because it requires more energy and because electricity is, in most cases, more expensive than fossil fuels. Photovoltaic water electrolysis may become more competitive as the cost continues to decrease with the technology advancement. The integration of solar energy concentration systems with systems capable of splitting water is of immense value and impact on the energetics and economics worldwide; by some is considered as the most important long-term goal in solar-fuel production to cut hydrogen costs and ensure virtually zero CO_2 emissions; however, the considerable use of small band gap semiconducting materials may cause serious life cycle environmental impacts. The utilization of an oxide semiconductor photocatalyst is a promising technique because the photocatalyst is in a solid phase form and is secure for use, resistant to deactivation, chemically stable, and

environmentally friendly. The diagram in Figure 2.1 shows that while the introduction of fuel cell technology will lead to a substantial reduction in the emissions of greenhouse gases (expressed in carbon units per kilometer), the use of fuel cells powered by hydrogen obtained from solar energy will reduce the emissions to nearly zero. Hydrogen is not present in nature in a gaseous form. However, it is abundantly available in plants, as well as in several compounds, such as methane, methanol, and higher hydrocarbons. Most importantly, it is available in water. Therefore, hydrogen must be extracted from these compounds.

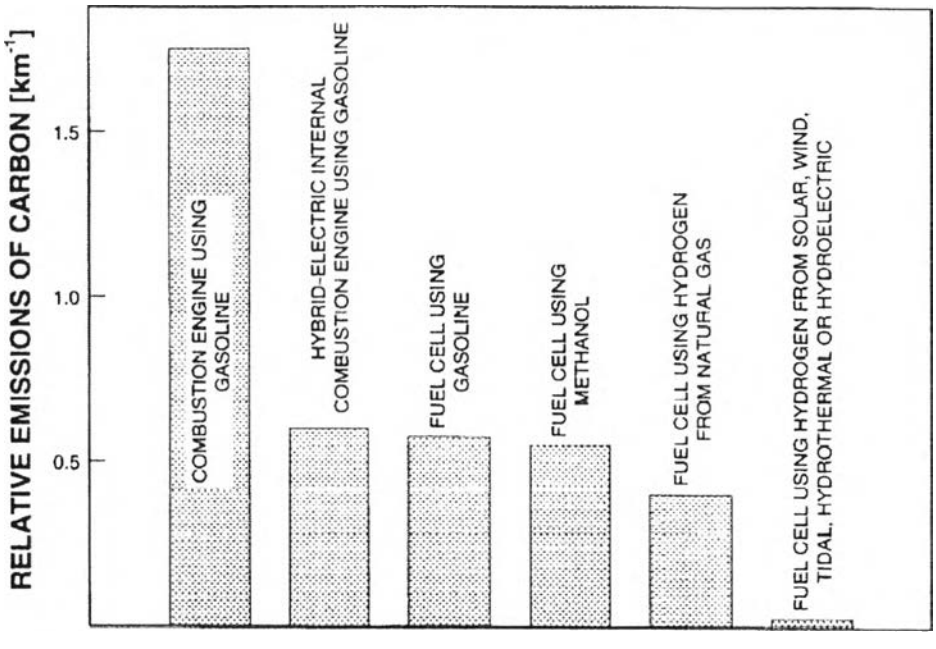

Figure 2.1 Relative emissions of greenhouse gases (expressed in carbon units per km) for vehicles powered by today's internal combustion engine using gasoline compared to vehicles powered by fuel cells (Bak *et al.*, 2002).

2.2 Water Splitting: Hydrogen Generation Using Solar Energy

2.2.1 Photocatalytic Reaction

Photocatalytic reactions have been extensively studied. Photocatalytic reactions are classified into two categories: "down-hill" and "up-hill" reactions. Degradation, such as photo-oxidation of organic compounds using oxygen molecules, is generally a down-hill reaction, of which the reaction proceeds irreversibly. In this

reaction, a photocatalyst works as a trigger to produce O_2^-, HO_2, OH•, and H^+ as active species for oxidation at the initial stage. This type of reaction is regarded as a photo-induced reaction, as depicted in Figure 2.2(a), and has been extensively studied using titanium dioxide photocatalyst (Fujishima *et al.*, 2000). On the other hand, water splitting reaction is accompanied by a largely positive change in the Gibbs free energy (ΔG^0 = 237 kJ/mol) and is an up-hill reaction. In this reaction, photon energy is converted into chemical energy, as also shown in Figure 2.2(b), similar to photosynthesis by green plants. Therefore, this type of reaction is called artificial photosynthesis.

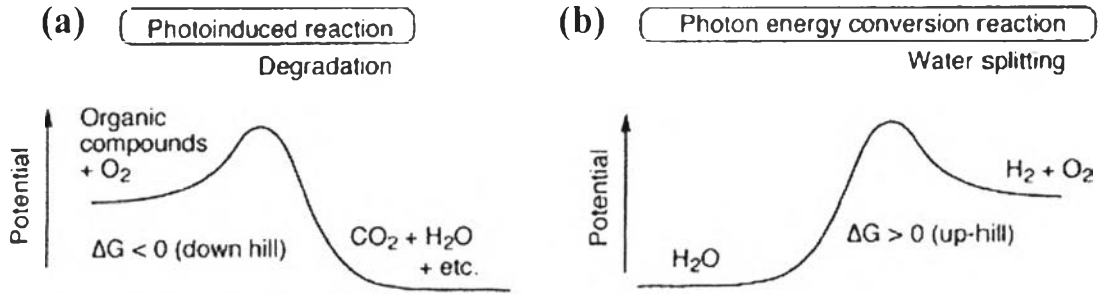

Figure 2.2 Types of photocatalytic reactions: (a) photoinduced reaction and (b) photon energy conversion reaction.

Since the first energy crisis in the early 1970s, much research has been devoted to the development of efficient systems that would enable the absorption and conversion of solar light into useful chemical energy resources. One of the most promising reactions of such ''artificial photosynthesis'' is the photocatalytic splitting of water to produce H_2 and O_2 under solar light:

$$H_2O \rightarrow H_2 + 1/2O_2,\ \Delta G^0 = 237.2\ \text{kJ/mol} \qquad (1)$$

The refinement of this up-hill reaction is greatly desired not only for the conversion and storage of solar energy but also for the clean and safe production of hydrogen since the consumption of hydrogen will be expected to increase dramatically, especially for use in fuel cells.

2.2.2 Splitting Water into Hydrogen

The technologies for hydrogen generation using sources of renewable energy are in the incubation stage. Photocatalytic splitting of water into hydrogen has attracted extensive attention due to its potential to obtain clean and highly efficient hydrogen energy from abundant water. For about 35 years, since the work of Fujishima and Honda, which reported on the photodecomposition of water over semiconductor photoelectrolysis cells (Fujishima *et al.*, 1972), many studies in the photocatalytic splitting of water have been carried out. The energy conversion efficiency of water photoelectrolysis is primarily determined by the properties of materials used for the photoelectrodes.

For photoelectrolysis of water, a potential difference of more than 1.23 eV is necessary between cathodic and anodic electrodes (Eq. (2)), where the following anodic and cathodic reactions take place simultaneously (Eq. (3) and (4)).

$$H_2O \rightarrow H_2 + 1/2O_2,\ E = 1.23\ eV \quad (2)$$

$$2H_2O + 2e^- \rightarrow H_2 + 2OH^-,\ E^0\ (pH = 7) = -0.41\ V\ vs.\ NHE \quad (3)$$

$$2H_2O \rightarrow O_2 + 4H^+ + 4e^-,\ E^0\ (pH = 7) = +0.82\ V\ vs.\ NHE \quad (4)$$

This potential difference is equivalent to the energy of a wavelength of approximately 1,008 nm. Therefore, if the energy of light is used effectively in an electrochemical system, it should be possible to decompose water with visible light of wavelength shorter than 1,008 nm. However, water is transparent to visible light, it cannot be decomposed by visible light alone. It can be split by irradiation alone only with ultraviolet light shorter than 190 nm. Fujishima and Honda (1972) were the first researchers to study photodecomposition of water over semiconductor photoelectrolysis cells using light of wavelength $\lambda < 400$ nm. Photoelectrolysis cells consisting of a TiO_2 electrode and a Pt back electrode are connected through an external load, as shown in Figure 2.3 Photo-irradiation of the TiO_2 electrode under a small electric bias leads to the evolution of H_2 and O_2 at the surface of the Pt electrode and TiO_2 electrode, respectively.

$$TiO_2 + 2h\nu \rightarrow 2e^- + 2h^+ \text{ (excitation of } TiO_2 \text{ by UV light)} \quad (5)$$

$$2h^+ + H_2O \rightarrow 1/2O_2 + 2H^+ \text{ (at the } TiO_2 \text{ electrode)} \quad (6)$$

$$2e^- + 2H^+ \rightarrow H_2 \text{ (at the Pt electrode)} \quad (7)$$

The overall reaction can be expressed as Eq. (7):

$$H_2O + h\nu \rightarrow 1/2O_2 + H_2 \quad (8)$$

Despite the successful work of Fujishima and Honda, the use of a photoelectrochemical cells involves the difficulty of constructing the oxide semiconductor photoelectrode. Therefore, applications of the principle of water photodecomposition using semiconductor for heterogeneous photocatalytic systems using powdered semiconductors instead of photoelectrodes have been actively studied by reason of their advantages over photoelectrochemical cells, i.e. low cost to construct, chemical stability under the light, and large surface area. Such attempts have been supported by two experimental advances. One is accumulation of data on photocatalytic reactions over powdered semiconductors, while the other is Bard's concept that can be pictured as a ''short-circuited'' photoelectrochemical cell, where semiconductor electrode and metal counter electrode have been brought into contact in single particle. The history and development of the briefly mentioned progress about water splitting can be traced as follows (Bard *et al.*, 1995).

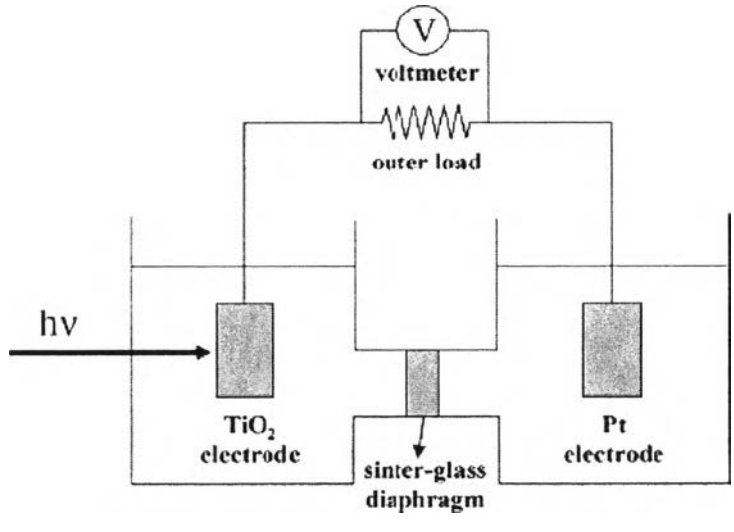

Figure 2.3 Electrochemical cell, in which a TiO_2 electrode is connected with a Pt electrode (Matsuoka *et al.*, 2007).

2.2.3 Efficiency

The free energy change for water splitting reaction is ΔG° = 237.2 kJ/mol or 2.46 eV/molecule of H_2O. Since two electrons are involved in the reaction, this corresponds to 1.23 eV/e, which is also the standard emf for the reaction. The photons in the solar spectrum provide sufficient energy to drive this reaction, but the efficiency of the reaction depends upon how the reaction is carried out. It is possible to cause water splitting thermally with light via concentrators and a solar furnace by heating water to 1,500-2,500 K. However, the efficiency of this process is typically below 2 %, and the cost of the capital equipment and material stability problems suggest that this approach for water splitting is not a promising one.

Since water itself does not absorb appreciable ration within the solar spectrum, one or more light-absorbing species, i.e. semiconductors as the photoconverters, must be used to transform the radiant energy to chemical (or electrical) energy in the form of electron/hole pairs, i.e. to the oxidizing and reducing potentials needed to drive the reaction. The maximum efficiency for photochemical water splitting has been considered in a number of papers and depends upon the band gap (or threshold energy), E_g, of the semiconductor. Radiation of energy below E_g is not absorbed while that above E_g is partly lost as heat by internal conversion or intraband thermalization processes. Additional thermodynamic losses occur because the excited state concentration is only a fraction of that of the ground state and because some excited states are lost through radiative decay (Archer *et al.*, 1990).

2.2.4 Semiconductor

A semiconductor is a material with an electrical conductivity that is intermediate between that of an insulator and a conductor. Like other solids, semiconductor materials have electronic band structure determined by the crystal properties of the material. The actual energy distribution among electrons is described by the Fermi level and temperature of the electrons. Among the bands filled with electrons, the one with the highest potential level is referred to as the valence band (VB), while the band outside of this is referred to as the conduction band (CB). The energy width of the forbidden band between the valence band and

the conduction band is referred to as the band gap (E_g). The overall structure of band gap energy is shown in Figure 2.4 The band gap can be considered as a wall that electrons must jump over in order to become free. When light is illuminated at appropriate wavelengths with energy equal or more than band gap energy, valence band (VB) electrons can move up to the conduction band (CB). At the same time, as many positive holes as the number of electrons that have jumped to the conduction band (CB) are created.

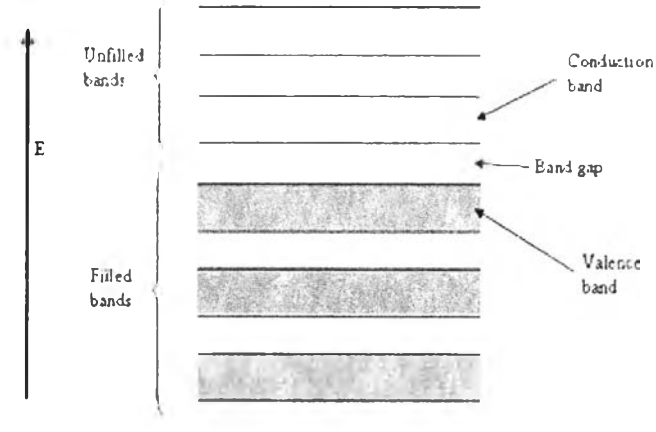

Figure 2.4 The structure of band gap energy.

2.2.5 Types of Semiconductor Systems Proposed for Solar Water Splitting

2.2.5.1 Semiconductor Solid State Photovoltaic Based Systems

A number of different approaches are possible with semiconductors. The most direct approach employs a solid state photovoltaic solar cell to generate electricity that is then passed into a commercial-type water electrolyzer, as shown in Figure 2.5(a). The electrolysis of water at a reasonable rate in a practical cell requires applied voltages significantly larger than the theoretical value (1.23 V at 25 °C). Moreover, the components are rugged and should be long-lived. The problem with such a system is its cost. Solar photovoltaics cannot currently produce electricity at competitive prices, and hydrogen from water electrolyzers is significantly more expensive than that produced chemically from coal or natural gas.

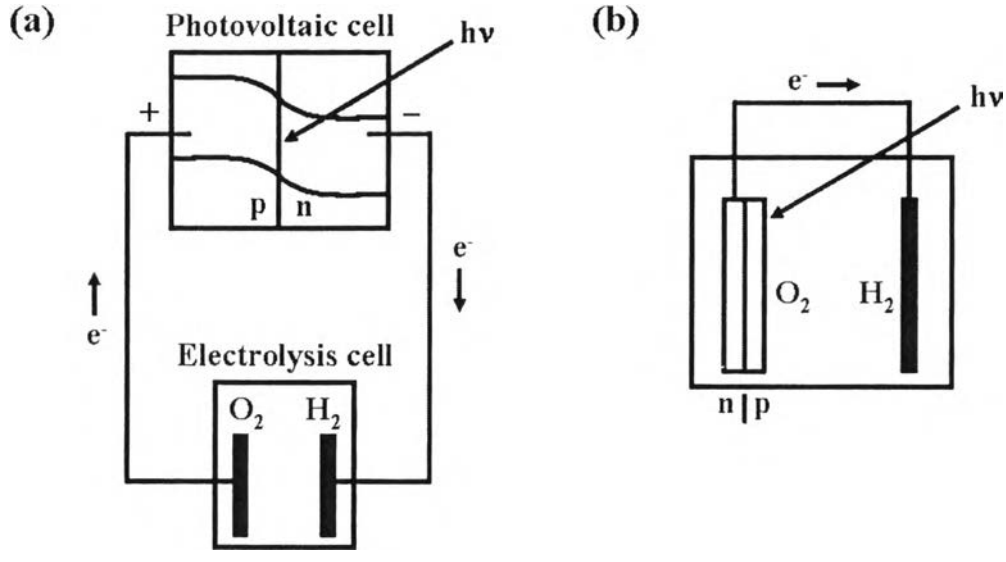

Figure 2.5 Schematic of (a) solid state photovoltaic cell driving a water electrolyzer and (b) cell with immersed semiconductor p/n junction (or metal/semiconductor Schottky junction) as one electrode.

An alternative system involves the semiconductor photovoltaic cell immersed directly in aqueous system, as illustrated in Figure 2.5(b). At the least, this eliminates the costs and mechanical difficulties associated with separate construction and interconnection of solar and electrochemical cells. In one such system, the electrodes are composed of single or multiple semiconductor p/n junctions that are irradiated while they are within the cell. This simpler apparatus is attained at the cost of encapsulating and coating the semiconductors to protect them from the liquid environment and probably with a more limited choice of electrocatalyst for H_2 or O_2 evolution. Note that, in addition to p/n semiconductor junctions, those between a metal and semiconductor (Schottky barriers) can also be used to produce a photopotential.

2.2.5.2 Semiconductor Electrode (Liquid Junction) Systems

Of more interest are systems, in which the photopotential to drive the water splitting reaction is generated directly at the semiconductor/liquid interface, as shown in Figure 2.6. Rather extensive research was carried out on various metal electrodes, sometimes covered with oxide or other films, and immersed

in a variety of solutions, including some containing fluorescent dyes. The discovery of the transistor and interest in semiconductor materials led to more extensive electrochemical and photoelectrochemical studies, usually with the goal of characterizing the semiconductor.

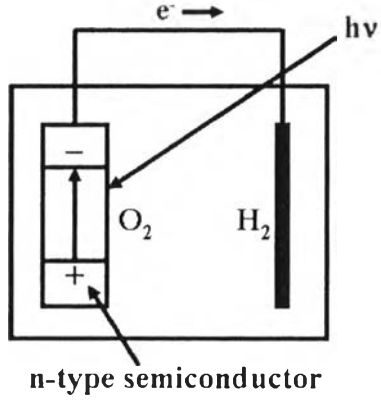

Figure 2.6 Schematic of liquid junction semiconductor electrode cell.

The modern era of semiconductor electrodes and interest in these in photoelectrochemical devices for energy conversion, especially via the water splitting reaction, can be cited to the work of Fujishima and Honda on single-crystal TiO_2 electrodes (Fujishima and Honda 1972). Indeed, water splitting in TiO_2-based cells can be accomplished, but only with an additional electrical bias. The problem with TiO_2 is that the conduction band is too low, i.e. at an insufficiently negative potential, to generate hydrogen at a useful rate. Moreover, because the TiO_2 band gap is too large (3.2 eV for anatase and 3.0 eV for rutile), only a small fraction of the solar light is absorbed. Cells with TiO_2 electrodes of various types, e.g. single crystal, polycrystal, and thin film, have nevertheless been heavily investigated, largely because TiO_2 is very stable and is a good model for understanding the semiconductor/liquid interface.

2.2.5.3 Semiconductor Particle Systems

A considerable simplification of the apparatus is possible if the electrochemical cell can be replaced by simple dispersions of semiconductor particles. In such dispersions, the semiconductor particles can be coated with islands of metals or metal oxides that behave as catalytic sites, with each particle behaving

as a microelectrochemical cell, as shown in Figure 2.7. TiO_2 has been a favorite material, although other compounds, such as CdS and ZnO, have also been studied. While a number of interesting photoreactions have been carried out, including the use of particles to destroy organics and to plate metals from wastewater (Ollis and Al-Ekabi, 1993) and for synthetic purposes (Serpone and Pelizzetti, 1989), various reports on the use of particulate systems for water splitting remain controversial. An extension of this approach is the use of colloidal-sized particles down to nanoparticles. Such small particles also have very high surface areas that, in principle, allow faster capture of the photogenerated charges by solution species and with less bulk recombination.

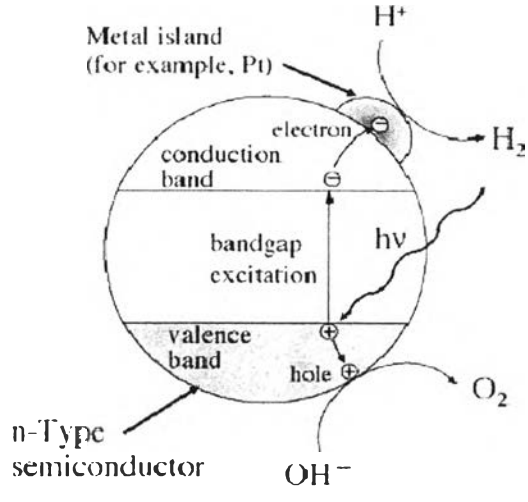

Figure 2.7 Representation of semiconductor particulate systems for heterogeneous photocatalysis (Matsuoka *et al.*, 2007).

2.2.6 The Principle of Water Splitting Using Semiconductor Particle

The principle of water splitting using a semiconductor photocatalyst is shown in Figure 2.8. The semiconductor photocatalyst absorbs impinging photons with energies equal to or higher than its band gap or threshold energy. Each photon of the required energy (i.e. wavelength) that strikes an electron in the occupied valence band (VB) of the semiconductor atom can elevate that electron to the unoccupied conduction band (CB), leading to excited state conduction band electrons and positive valence band holes (Serpone and Pelizzetti, 1989). The photogenerated

electrons and holes cause redox reactions similar to electrolysis. Water molecules are reduced by the electrons to form H_2 and oxidized by the holes to form O_2, leading to overall water splitting. The width of the band gap and the potentials of the conduction and valence bands are important for the semiconductor photocatalyst material. The bottom level of the conduction band (CB) has to be more negative than the reduction potential of H^+/H_2 (0 V vs NHE), while the top level of the valence band (VB) has to be more positive than the oxidation potential of O_2/H_2O (1.23 V).

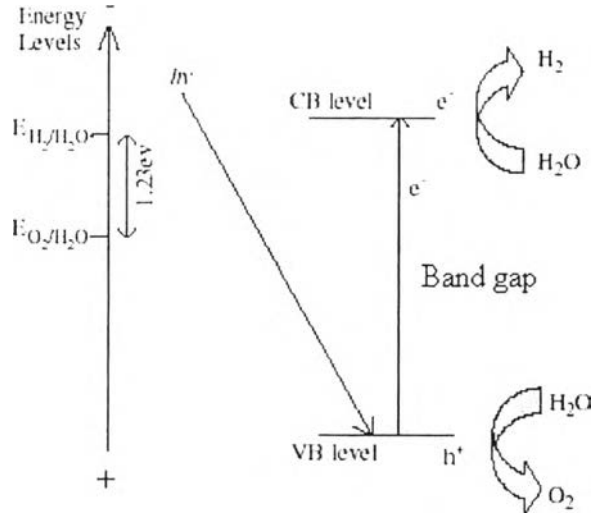

Figure 2.8 Reaction schematic for water splitting reaction over semiconductor photocatalysts.

The competition between charge carrier recombination and charge carrier trapping followed by the competition between recombination of trapped carriers and interfacial charge transfer are what determine the overall quantum efficiency for interfacial charge transfer. Also of great importance are the band positions or flat band potentials of the semiconductor material. These indicate the thermodynamic limitations for the photoreactions that can take place.

However, the potential of the band structure is just the thermodynamic requirement. Other factors, such as charge separation, mobility, and lifetime of photogenerated electrons and holes, also affect the photocatalytic properties, as shown in Figure 2.9, in which the fate of these charge carriers may take different

paths. Firstly, they can get trapped in the bulk either in shallow or in deep traps. Secondly, they can recombine, non-radiatively or radiatively, dissipating the input energy as heat. Finally, they can react with electron donors or acceptors adsorbed on the surface of the photocatalyst (Hoffmann *et al.*, 1995). These properties are strongly influenced by bulk properties of the material, such as crystallinity. Surface properties, such as surface area and active reaction sites, are also imperative. Cocatalysts, such as Pt and NiO, are often loaded on the photocatalyst surface in order to introduce active sites for H_2 evolution. Thus, suitable bulk and surface properties and energy structure are demanded for photocatalysts. So, one can state that the photocatalyst is a highly functional material.

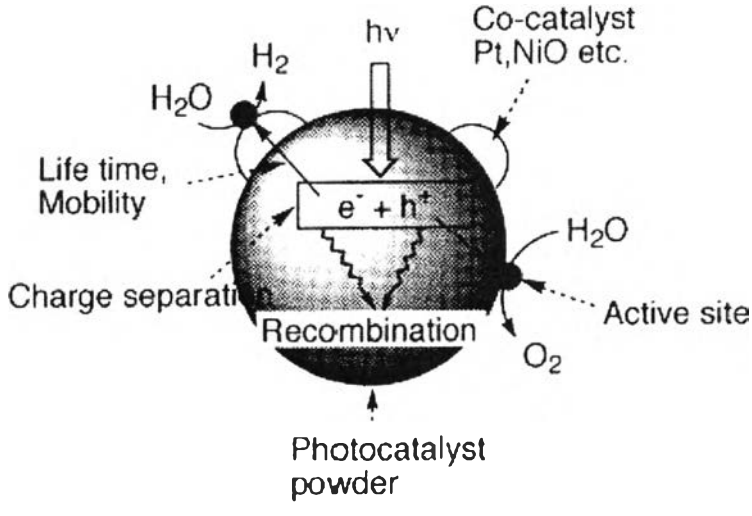

Figure 2.9 Processes occurring in semiconductor photocatalyst under photoexcitation for water splitting reaction.

2.3 Photocatalyst

Since water is transparent to solar radiation, direct decomposition of water by solar light is not viable. Energetically, it seems relatively easy to photocatalyze water, since the theoretical minimum photovoltage required for this process is only 1.23 eV. Semiconductors, in the presence of light energy, are capable of decomposing water into hydrogen and oxygen depending upon energy levels of their conduction and valence bands. In an ideal system, conduction band level should be

well above (more negative than) the water reduction level, and valence band edge should be well below (more positive than) the water oxidation level for an efficient production of hydrogen and oxygen from water by photolysis, as shown in Figure 2.10. Some of the photocatalysts that satisfy both conditions are TiO_2, $SrTiO_3$, $CaTiO_3$, $Sr_2Nb_2O_5$, $Sr_2Ta_2O_7$, ZnO, CdS, NiO, etc.

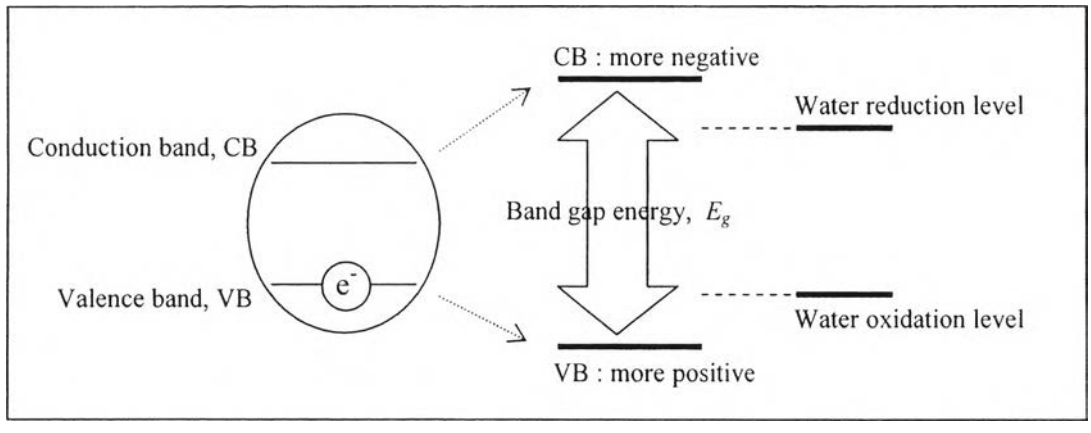

Figure 2.10 Band gap energy of the photocatalyst.

Powders with semiconductor characteristics have been widely employed in photocatalytic systems because they are capable of generating charge carriers by absorbing photon energies. The separation effectiveness of the photo-induced charge carriers is an important factor in determining the photocatalytic activity of the powders. Among the photocatalysts investigated, TiO_2 is the most widely used semiconductor photocatalyst for various photocatalytic systems (Fujima *et al.*, 2000; Chen and Mao, 2007)

2.4 Titanium Oxide Photocatalyst

2.4.1 General Remarks

Titanium dioxide (TiO_2) belongs to the family of transition metal oxides TiO_2 has received a great deal of attention due to its chemical stability, non-toxicity, low cost, and other advantageous properties. Particularly, TiO_2 is extensively utilized in solar energy conversion, i.e. solar cell, and photocatalysis applications (Hoffmann *et al.*, 1995). As a result of its high refractive index, it is

used as anti-reflection coating in silicon solar cells and in many thin film optical devices. TiO_2 is successfully used as gas sensor (due to the dependence of the electric conductivity on the ambient gas composition) and is utilized in the determination of oxygen and carbon monoxide concentrations at high temperatures (> 600°C), by simultaneously determining CO/O_2 and CO/CH_4 concentrations (Savage *et al.*, 2001). Due to its hemocompatibility with the human body, TiO_2 is also used as a biomaterial (as bone substituent and reinforcing mechanical supports).

2.4.2 Crystal Structure and Properties

The main four polymorphs of TiO_2 found in nature are anatase (tetragonal), brookite (orthorhombic), rutile (tetragonal), and TiO_2 (B) (monoclinic). The structures of rutile, anatase, and brookite can be discussed in terms of (TiO_2^{6-}) octahedrals. The three crystal structures differ by the distortion of each octahedral and by the assembly patterns of the octahedral chains. Anatase can be regarded to be builtup from octahedrals that are connected by their vertices; in rutile, the edges are connected; and in brookite, both vertices and edges are connected, as shown in Figure 2.11 (Carp *et al.*, 2004).

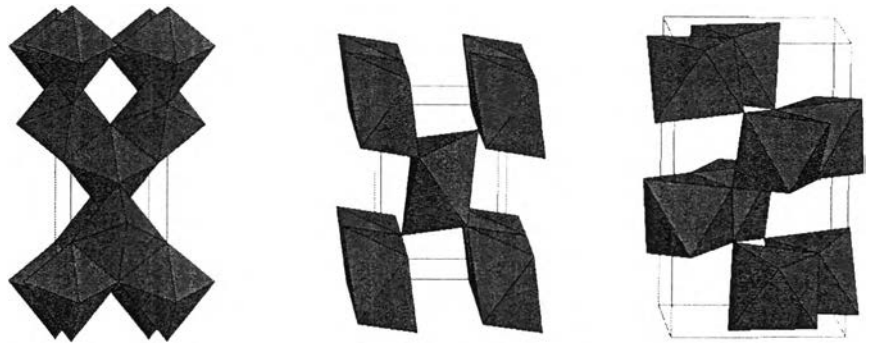

(a) (b) (c)

Figure 2.11 Crystal structures of (a) anatase, (b) rutile, and (c) brookite.

Thermodynamic calculations based on calorimetric data predict that rutile is the most stable phase at all temperatures and pressures up to 60 kBar. The small differences in the Gibbs free energy (4-20 kJ/mol) among the three phases

suggest that the metastable polymorphs are almost as stable as rutile at normal pressures and temperatures. Particle size experiments affirm that the relative phase stability may reverse when particle sizes decrease to sufficiently low values due to surface energy effects (surface free energy and surface stress, which depend on particle size). If the particle sizes of the three crystalline phases are equal, anatase is the most thermodynamically stable at sizes less than 11 nm, brookite is the most stable between 11 and 35 nm, and rutile is the most stable at sizes greater than 35 nm (Zhang and Banfield, 2000).

The enthalpy of the anatase-rutile phase transformation is low. However, there are widespread disagreement in the value, which ranges from -1.3 to -6.0 ± 0.8 kJ/mol. Kinetically, anatase is stable, i.e. its transformation into rutile at room temperature is so slow that the transformation practically does not occur. At macroscopic scale, the transformation reaches a measurable speed for bulk TiO_2 at temperature greater than 600°C. During the transformation, anatase pseudoclose-packed planes of oxygen are retained as rutile close-packed planes, and a co-operative rearrangement of titanium and oxygen ions occurs within this configuration. The proposed mechanism implies at least spatial disturbance of the oxygen ion framework and a minimum breaking of Ti–O bonds as a result of surface nucleation and growth. The nucleation process is very much affected by the interfacial contact in nanocrystalline solids, and once initiated, it quickly spreads out and grain growth occurs (Ding and Liu, 1998).

The anatase-rutile transformation has been studied for both mechanistic and application-driven reasons, because the TiO_2 phase (i.e. anatase or rutile) is one of the most critical parameters determining the use as a photocatalyst, catalyst, or as ceramic membrane material. This transformation, achieved by increased temperature or pressure, is influenced by several factors, such as concentration of lattice and surface defects, particle size, and applied temperature and pressure.

In photocatalysis applications, both crystal structures, i.e. anatase and rutile, are commonly used, with anatase showing a greater photocatalytic activity for most reactions. It has been suggested that this increased photoreactivity is due to

anatase's slightly higher Fermi level, lower capacity to adsorb oxygen, and higher degree of hydroxylation (i.e. number of hydroxyl groups on the surface). Reactions, in which both crystalline phases have the same photoreactivity (Deng *et al.*, 2002) or rutile exhibiting a higher one (Mills *et al.*, 2003), are also reported. Furthermore, there are also studies, which claim that a mixture of anatase (70-75 %) and rutile (30-25 %) is more active than pure anatase (Mugglie and Ding, 2001). The disagreement of the results may lie in the intervening effect of various coexisting factors, such as specific surface area, pore size distribution, crystal size, and preparation methods, or in the way the activity is expressed. The behavior of Degussa P-25 commercial TiO_2 photocatalyst, consisting of a mixture of anatase and rutile in an approximate proportion of 80/20, is for many reactions more active than both the pure crystalline phases. The enhanced activity arises from the increased efficiency of the e^-/h^+ separation due to the multiphase nature of the particles. Water splitting reaction is a special case because band bending is necessary in order to reduce and oxidize water.

2.4.3 Semiconductor Characteristic and Photocatalytic Activity

Due to oxygen vacancies, TiO_2 is an n-type semiconductor. A semiconductor photocatalyst is characterized by its capability to adsorb simultaneously two reactants, which can be reduced and oxidized by a photonic activation through an efficient absorption ($h\nu \geq E_g$). The ability of a semiconductor to undergo photoinduced electron transfer to an adsorbed reactant is governed by the band energy positions of the semiconductor and the redox potential of the adsorbates. The energy level at the bottom of conduction band is actually the reduction potential of photoelectrons. The energy level at the top of valence band determines the oxidizing ability of photogenerated holes, each value reflecting the ability of the system to promote reductions and oxidations. The flat band potential (V_{fb}) locates the energy of both charge carrie rs at the semiconductor-electrolyte interface, depending on the nature of the material and system equilibrium. From the thermodynamic point of view, adsorbed couples can be reduced photocatalytically by conduction band electrons if they have more positive redox potentials than V_{fb} of the conduction band, and can be oxidized by valence band holes if they have more negative redox potentials than V_{fb} of the valence band (Rajeshwar, 1995).

Unlike metals, semiconductors lack a continuum of interband states to assist the recombination of electron-hole (e^-/h^+) pairs, which assure a sufficiently long life time of the pairs to diffuse to the photocatalyst surface and initiate a redox reduction. The differences in lattice structures of anatase and rutile TiO_2 cause different densities and electronic band structures, leading to different band gaps (for bulk materials: anatase 3.20 eV and rutile 3.02 eV). Therefore, the absorption thresholds correspond to wavelengths of 384 and 410 nm for the two TiO_2 forms, respectively. The mentioned values concern single crystals or well-crystallized samples. Higher values are usually obtained for weakly crystallized thin films or nanosized materials. The blue shift of the fundamental absorption edge in TiO_2 nanosized materials has been observed, amounting to 0.2 eV for crystallite sizes in the range of 5-10 nm.

As mentioned, TiO_2 has been most widely used for studies of photocatalytic decomposition of water, because of its high stability against photocorrosion and its favorable band gap energy. Presently, the energy conversion efficiency from solar to hydrogen by TiO_2 photocatalytic water splitting is still low, mainly due to the following reasons:

- Recombination of photo-generated electron/hole pairs: CB electrons can recombine with VB holes very quickly and release energy in the form of unproductive heat or photons;
- Fast backward reaction: Decomposition of water into hydrogen and oxygen is an energy increasing process, thus backward reaction (recombination of hydrogen and oxygen into water) easily proceeds;
- Inability to utilize visible light: The band gap of TiO_2 is about 3.2 eV, and only UV light can be utilized for hydrogen production. Since the UV light only accounts for about 4 % of the solar radiation energy while the visible light contributes about 45 %, the inability to utilize visible light limits the efficiency of solar photocatalytic hydrogen production.

In order to resolve the above listed problems and make solar photocatalytic hydrogen production feasible, continuous efforts have been made to promote the photocatalytic activity and enhance the visible light response. Addition of electron donors (hole scavengers), addition of carbonate salts, noble metal loading,

metal ion doping, anion doping, dye sensitization, composite semiconductors, metal ion-implantation, etc. have been investigated, and some of them have been proved to be useful to enhance hydrogen production. The above listed techniques influencing H_2 production have been grouped under two broad classifications, i.e. 'chemical additives' and 'photocatalyst modification techniques'.

2.5 Nano-Photocatalyst

2.5.1 General Remarks

Nanocrystalline photocatalysts are ultra-mall semiconductor particles, which are few nanometers in size. During the past decade, the photochemistry of nanosized semiconductor particles has been one of the fastest growing research areas in physical chemistry. The interest in these small semiconductor particles originates from their unique photophysical and photocatalytic properties. Several review articles have been published concerning the photophysical properties of nanocrystalline semiconductors. Such studies have demonstrated that some properties of nanocrystalline semiconductor particles are in fact different from those of bulk materials.

Nanosized particles possess properties with fall into the region of transition between the molecular and bulk phases. In the bulk material, the electron excited by light absorption funds a high density of states in the conduction band, where it can exist with different kinetics energies. In the case of nanoparticles, however, the particle size is the same as or smaller than the size of the first excited state. Thus, the electrons and holes generated upon illumination cannot suit into such a particle, unless they assume a state of higher kinetics energy. Hence, as the size of the semiconductor particle is reduced below a critical diameter, the spatial confinement of the charge carriers within a potential well, like ''a particle in a box'', causes them to mechanically behave quantum. In solid state terminology, this means that the bands split into discrete electronic states (quantized levels) in the valence and conduction bands, and the nanoparticle progressively behaves similar to a giant atom. Nanosized semiconductor particles, which exhibit size-dependent optical and electronic properties, are called quantized particles or quantum dots (Kamat, 1995).

2.5.2 Activity of Nano-Photocatalyst

One of the main advantages of the application of nanosized particles is the increase in the band gap energy with decreasing particle size. As the size of a semiconductor particle falls below the critical radius, the charge carriers begin to behave mechanically quantum, and the charge confinement leads to a series of discrete electronic states. As a result, there is an increase in the effective band gap and a shift of the band edges. Thus, by varying the size of the semiconductor particles, it is possible to enhance the redox potential of the valence band holes and the conduction band electrons.

However, the solvent reorganizational free energy for charge transfer to a substrate remains unchanged. The increasing driving force and the unchanged solvent reorganizational free energy are expected to lead to an increase in the rate constants for charge transfer at the surface. The use of nanosized semiconductor particles may result in increased photocatalytic activity for systems, in which the rate-limiting step is interfacial charge transfer. Hence, nanosized semiconductor particles can possess enhanced photoredox chemistry with reduction reactions, which might not otherwise proceed in bulk materials, being able to occur readily using sufficiently small particles. Another factor, which could be advantageous, is the fact that the fraction of atoms that are located at the surface of a nanoparticle is very large. Nanosized particles also have high surface area-to-volume ratio, which further enhances their catalytic activity. One disadvantage of nanosized particles is the need for light with a shorter wavelength for photocatalyst activation. Thus, a smaller percentage of a polychromatic light source will be useful for photocatalysis.

In large TiO_2 particles (Zhang *et al.*, 1998), volume recombination of the charge carriers is the dominant process and can be reduced by a decrease in particle size. This decrease also leads to an increase in the surface area, which can be translated as an increase in the available surface active sites. Thus, a decrease in particle size should also result in higher photonic efficiencies due to an increase in the interfacial charge carrier transfer rates. However, as the particle size is lowered below a certain limit, surface recombination processes become dominant, since firstly most of the electrons and holes are generated close to the surface, and secondly surface recombination is faster than interfacial charge carrier transfer

processes. This is the reason why there exists an optimum particle size for maximum photocatalytic efficiency.

2.6 Chemical Additive for Enhancement of Photocatalytic H_2 Production

Due to rapid recombination of photogenerated CB electrons and VB holes, it is difficult to achieve water splitting for hydrogen production using TiO_2 photocatalyst in pure distilled water. Adding electron donors (sacrificial reagents or hole scavengers) to react irreversibly with the photogenerated VB holes can enhance the electron/hole separation, resulting in higher quantum efficiency. Since electron donors are consumed in photocatalytic reaction, continual adding of electron donors is required to sustain hydrogen production.

Organic compounds, especially hydrocarbons, are widely used as electron donors for photocatalytic hydrogen production as they can be oxidized by VB holes. The remaining strong reducing CB electrons can reduce protons to hydrogen molecules. EDTA, methanol, ethanol, CN^-, lactic acid, and formaldehyde have been tested and proved to be effective to enhance hydrogen production. Nada *et al.* (2005) carried out a qualitative investigation to study the effects of different electron donors on hydrogen production. The rankings in terms of the degree of hydrogen production enhancement capability were found to be: EDTA > methanol > ethanol > lactic acid. It should be noted that the decomposition of these hydrocarbons could also contribute to a higher hydrogen yield since hydrogen is one of their decomposed products.

Other inorganic ions, such as S^{2-}/SO_3^{2-}, Ce^{4+}/Ce^{3+}, and IO_3^-/I^-, were also used as sacrificial reagents for hydrogen production. When CdS is used as photocatalyst for hydrogen production from water splitting, photocorrosion occurs as follows:

$$CdS + 2h^+ \rightarrow Cd^{2+} + S \quad (9)$$

By serving as a sacrificial reagent, S^{2-} can react with 2 holes to form S. The aqueous SO_3^{2-} added can dissolve S into $S_2O_3^{2-}$ in order to prevent any detrimental deposition of S onto CdS. Therefore, photocorrosion of CdS is prevented. In another system of using inorganic ions, I^- (electron donor) and IO_3^- (electron acceptor) work as a pair of

redox mediators. Two photocatalysts were employed to produce H_2 and O_2 under the mediation of I^- and IO_3^-, respectively. For hydrogen production on the photocatalyst with more negative CB level, I^- can scavenge holes and, thus, CB electrons are available to reduce protons to hydrogen molecules. For oxygen production on the photocatalyst with more positive VB level, IO_3^- can react with CB electrons to form I^- and, thus, VB holes can oxidize water to oxygen. In this system, photocatalytic water splitting produces both hydrogen and oxygen without consumption of the sacrificial reagent, as illustrated in Figure 2.12. As rutile has unique selectivity in oxidation, oxygen molecules are evolved. For comparison, IO_3^- anions are produced on the surface of anatase. Therefore, the combination of anatase and rutile shows a higher hydrogen production rate under the mediation of I^-/IO_3^- pairs. Similarly, Ce^{4+}/Ce^{3+} and Fe^{3+}/Fe^{2+} pairs are also effective for water splitting hydrogen production.

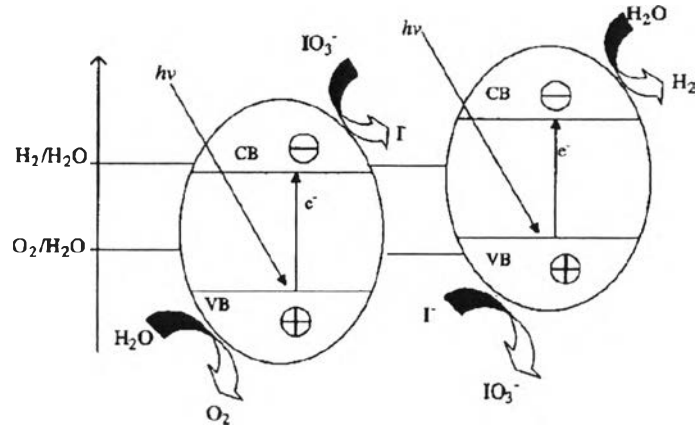

Figure 2.12 Photocatalytic hydrogen production over anatase/rutile TiO_2 under the mediation of I^-/IO_3^-.

2.7 Metal Loading for Enhancement of H_2 Production

Noble and transition metals, including Pt, Au, Pd, Rh, Ni, Cu, and Ag, have been reported to be very effective for enhancement of TiO_2 photocatalysis. As the Fermi levels of these metals are lower than that of TiO_2, photoexcited electrons can be transferred from conduction band to metal particles deposited on the surface of TiO_2, while photogenerated valence band holes remain on the TiO_2. These activities greatly reduce the possibility of electron-hole recombination, resulting in efficient separation and stronger photocatalytic reactions. As electrons accumulate on the metal particles, their Fermi levels shift closer to the conduction band of TiO_2, resulting in more negative energy levels. This is beneficial for water splitting for hydrogen production. Furthermore, smaller metal particles deposited on TiO_2 surface exhibit more negative Fermi level shift. Accumulated electrons on metal particles can then be transferred to protons adsorbed on the surface and further reduce the protons to hydrogen molecules. Therefore, these metals with suitable work function can help electron transfer, leading to higher photocatalytic activity. Bamwenda *et al.* (1995) compared hydrogen production from water-ethanol solution using Au-loaded TiO_2 and Pt-loaded TiO_2 as photocatalysts. It was found that loading of Pt worked better than loading of Au. Sakthivel *et al.* (2004) investigated photooxidation of Acid Green 16 using Pt, Au, and Pd-loaded TiO_2 as photocatalysts. Optimal loading was observed in their experiments. Too much metal particle deposition might reduce photon absorption by TiO_2 and might also become electron-hole recombination centers, resulting in lower efficiency. Loadings of Pt and Au were more effective than loading of Pd because of suitable electron affinity and work function of Pt and Au. It should be noted that although the metal loading can reduce recombination to some extent, hydrogen production from pure water splitting is difficult to achieve, because: (i) recombination cannot be completely eliminated; and (ii) backward reaction of H_2 and O_2 to form H_2O is thermodynamically favorable. Therefore, as discussed in the previous section, electron donors, as well as other mediators, are required to avoid the above listed problems. Since Pt is very expensive, more research is needed to identify low-cost metals with acceptable enhancement of photocatalytic activity. For example, Dhanalakshimi *et al.* (2000) investigated dye-

sensitized hydrogen production. When Pt/TiO_2 and Cu/TiO_2 were used as photocatalysts, enhanced hydrogen production was observed, and the effect of Cu loading was almost comparable to Pt loading. Unlike dye sensitization, Wu and Lee (2004) deposited Cu particles on TiO_2 surface for hydrogen production from methanol solution. At the optimal loading of Cu, hydrogen production rate was enhanced as much as 10 times higher. Other low-cost metals, such as Ni and Ag, were also found to be effective for photocatalytic activity enhancement. These low-cost but effective metals are expected to be promising materials to improve photocatalytic activities of TiO_2 for practical applications. For photocatalytic hydrogen production, Pt is mostly considered by several researchers to be the most effective cocatalyst and is widely used, resulting in considerably high H_2 evolution efficiency.

2.8 Ion Doping for Enhancement of H_2 Production

2.8.1 Metal Ion Doping

Transition metal ion doping and rare earth metal ion doping have been extensively investigated for enhancing the TiO_2 photocatalytic activities. Hoffmann *et al.* (1995) carried out a systematic investigation to study the photoreactivity of 21 metal ions doped into TiO_2. It was found that doping of metal ions could expand the photo-response of TiO_2 into visible spectrum. As metal ions are incorporated into the TiO_2 lattice, impurity energy levels in the band gap of TiO_2 are formed, as indicated below:

$$M^{n+} + h\nu \rightarrow M^{(n+1)+} + e^-_{cb} \quad (10)$$

$$M^{n+} + h\nu \rightarrow M^{(n-1)+} + h^+_{vb} \quad (11)$$

where M and M^{n+} represent metal and metal ion dopant, respectively. Furthermore, electron and hole transfer between metal ions and TiO_2 can alter electron/hole recombination as:

$$\text{Electron trap}: \quad M^{n+} + e^-_{cb} \rightarrow M^{(n-1)+} \quad (12)$$

$$\text{Hole trap}: \quad M^{n+} + h^+_{vb} \rightarrow M^{(n+1)-} \quad (13)$$

The energy level of $M^{n+}/M^{(n-1)+}$ should be less negative than that of the conduction (CB) edge of TiO_2, while the energy level of $M^{n+}/M^{(n+1)+}$ should be less positive than that of the valance band (VB) edge of TiO_2. For photocatalytic reactions, carrier transferring is as important as carrier trapping. Only if the trapped electron and hole are transferred to the surface, photocatalytic reactions can occur. Therefore, metal ions should be doped near the surface of TiO_2 particles for a better charge transferring. In case of deep doping, metal ions likely behave as recombination centers, since electron/hole transferring to the interface is more difficult. Furthermore, there exists an optimum concentration of doped metal ion, above which the photocatalytic activity decreased due to the increase in recombination. Among the 21 metal ions studied, Fe, Mo, Ru, Os, Re, V, and Rh ions can increase photocatalytic activity, while Co and Al ions caused detrimental effects. The different effects of metal ions result from their abilities to trap and transfer electrons/holes. For example, Cu and Fe ions can trap not only electrons but also holes, and the impurity energy levels introduced are near the conduction band, as well as valance band edges of TiO_2. Therefore, doping of either Cu or Fe ions could be recommended for enhancement of photocatalytic activity.

Peng *et al.* (2004) investigated the effect of Be ion-doped TiO_2 on photocatalytic hydrogen production in the presence of ethanol as electron donor. It was found that the Be ion doping near the surface was beneficial for charge carrier transferring, while deep doping led to poor performance. Furthermore, doping content and preparation methods could also affect photocatalytic hydrogen production. Under optimal condition of Be ion doping into TiO_2, hydrogen production was found to be 75 % higher than that of un-doped TiO_2. Extensive research on metal ion doping method for enhancement of TiO_2 photocatalytic activities has been carried out, especially for water/air cleaning applications. Organic compounds adsorbed by the photocatalysts are decomposed mainly by the valence band holes and radicals induced by holes. Therefore, the mechanism involved in transferring these photogenerated holes to the interface is of paramount importance. On the other hand, for photocatalytic hydrogen production, the transfer of conduction band electrons to the interface and their energy levels are the most important factors that affect the hydrogen production rate. Hence, the results based on water/air

cleaning applications cannot be directly applied to hydrogen production. Besides, the TiO_2 photocatalytic effect is very sensitive to the metal ion doping method, doping content, and doping depth. Therefore, a systematically comparative investigation is needed in order to characterize photocatalytic hydrogen production enhanced by metal ion doping.

2.8.2 Anion Doping

The use of anion doping to improve hydrogen production under visible light is rather a new method with few investigations reported in open literature. Doping of anions (N, F, C, S, etc.) in TiO_2 crystal could shift its photo-response into visible spectrum. Unlike metal ions (cations), anions less likely form recombination centers and, therefore, are more effective to enhance the photocatalytic activity. Asahi *et al.* (2001) determined the substitutional doping contents of C, N, F, P, and S for O in anatase TiO_2. It was found that mixing of p states of N with 2p of O could shifts VB edge upwards to narrow down the band gap of TiO_2. Although doping of S had resulted in a similar band gap narrowing, the ionic radius of S was reported to be too large to be incorporated into the lattice of TiO_2. Doping of C and P was found to be less effective as the introduced states were so deep that photogenerated charge carriers were difficult to be transferred to the surface of the catalyst.

The N-doped TiO_2 thin film was prepared by sputtering TiO_2 in an N_2 (40 %)/Ar gas mixture, followed by annealing at 550°C in N_2 for about 4 h. N-doped TiO_2 powder was also prepared by treating TiO_2 in NH_3 (67 %)/Ar at 600°C for 3 h. The N-doped TiO_2 was reported to be effective for methylene blue decomposition under visible light ($\lambda > 400$ nm). Additionally, it was reported by Umebayashi *et al.* (2002) that S-doped TiO_2 could be prepared by annealing of TiS_2. When annealed at 600°C, TiS_2 was partly changed to anatase TiO_2. The residual S atoms in the anatase TiO_2 formed S-doped TiO_2 by Ti–S bonds. Band structures of the S-doped TiO_2 were calculated using the super cell approach. It was found that when TiO_2 was doped with S, the mixing of S3p states with the valance band of TiO_2 increased the width of valence band, resulting in band gap narrowing. Since the band gap narrowing was caused by valence band upward shifting, the conduction band remained unchanged.

Therefore, the S-doped TiO_2 should be able to reduce protons for hydrogen production under visible light. On the other hand, the upward shift of valence band may reduce the oxidation ability under visible light. Ohno *et al.* (2004) developed a new method to prepare S-doped TiO_2 powder. Titanium isopropoxide was mixed with thiourea in ethanol and stirred. After subsequent evaporation, aging, and calcination, S-doped TiO_2 powder was obtained. The S ions were incorporated to replace some of the Ti atoms in the form of S^{4+}. The photocatalytic activity of S-doped TiO_2 was then evaluated by photodecomposition of 2-propanol and methylene blue. It was reported that S-doped TiO_2 worked better than pure TiO_2 under visible light irradiation. Although the valence band was shifted upwards, the oxidation ability was found to be still high. Other anions, such as C and F ions, have also been investigated and found to be able to expand photo-response in visible spectrum.

Reddy *et al.* (2005) investigated the absorption of TiO_2, which is extended into the visible light region by doping with S, N, and C anions. The results showed that all anions could improve absorption of TiO_2 by reducing the band gap energy. The feature was more evident in N-doped TiO_2 compared to C and S because N-doped TiO_2 showed two band gap transitions. The first one was in the UV region (385 nm), which is accounted for the fundamental band transition of TiO_2, and the second in the visible region (495 nm), as a result of nitrogen doping. The distinction between two surface states was reflected as individualistic redox peaks. In contrast, the C- and S-doped samples did not show a sharp absorption edge as observed for pure TiO_2. This would imply that the doping introduces electronic states in the band gap that are spread across the band gap, resulting in a diffused absorption spectrum.

N-doped TiO_2 has been the most extensively investigated. The reported methods to dope N are heating of titanium hydroxide and urea, reactive DC magnetron sputtering, nitriding of anatase TiO_2 with alkylammonium salts, and treating TiO_2 powder in NH_3 (80 %)/Ar gas flow at 550°C. Similar to S-doping, N-doping also caused a valence band upward shift, resulting in a narrower band gap and less oxidating holes. Mrowetz *et al.* (2004) reported that N-doped TiO_2 was unable to oxidize $HCOO^-$. However, for hydrogen production, electrons are responsible for reducing protons, and the ability of oxidation does not affect the

performance because the valence level of TiO_2 is far more positive than oxygen evolution energy level, and the conduction band remains almost unchanged after N-doping, being at a more negative than hydrogen production energy level. This throws a possibility that N-doped TiO_2 should be able to reduce protons for hydrogen production, although intensive research has not been investigated. Under visible light irradiation, electrons can be promoted from energy levels in the band gap formed by nitrogen doping to conduction band. However, electron-hole recombination possibility of N-doped TiO_2 was reported to be higher than undoped TiO_2 (Torres *et al.*, 2004).

Li *et al.* (2008) examined the UV-vis diffuse reflectance absorption spectra of TiO_2-300 °C and N-TiO_2-300 °C. It was observed that the absorption of TiO_2-300 °C was limited to UV light region, on the other hand, that of the N-TiO_2-300 °C was extended from 380 to 570 nm. The adsorption amount of EosinY on N-TiO_2 was about two times higher than that of TiO_2 at the same calcination temperature. Hence, the doped nitrogen can improve the adsorption of EosinY and accelerate the excited electron to transfer to the conduction band of N-TiO_2. Conclusively, for efficient photocatalytic reaction, coupling with other technologies, such as metal loading or electron donor addition, is necessary.

2.9 Dye Sensitization

Dye sensitization is widely used to utilize visible light for energy conversion. Some dyes having redox property and visible light sensitivity can be used in solar cells, as well as photocatalytic system (Gurunathan *et al.*, 1997). Under illumination by visible light, the excited dyes can inject electrons to CB of semiconductors to initiate the catalytic reactions, as illustrated in Figure 2.13. Even without semiconductors, some dyes, for example safranine O/EDTA and T/EDTA, are able to absorb visible light and produce electrons as reducing agents strong enough to produce hydrogen (Bi and Tien, 1984). Nevertheless, without semiconductors acting as efficient charge seperators, the rate of hydrogen production merely by dyes is very low.

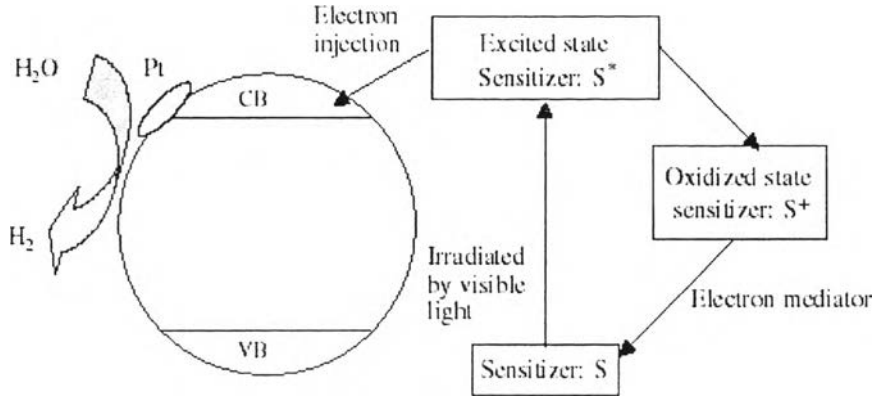

Figure 2.13 Mechanism of dye-sensitized photocatalytic hydrogen production under visible light irradiation.

High hydrogen production rate can be obtained by efficient absorption of visible light and efficient transfer of electrons from excited dyes to CB of TiO_2. The CB electrons can then be transferred to metal particles (such as Pt) loaded on surface to initiate water reduction. In order to regenerate dyes, electron donors or sacrificial agents, such as I_3^-/I^- pair and EDTA, can be added to the solution to sustain the reaction cycle. The excitation, electron injection, and dye regeneration can be expressed as follows:

$$dye + h\nu \rightarrow dye^* \quad (14)$$

$$dye^* + TiO_2 \rightarrow dye^+ + e^- \quad (15)$$

$$dye^+ + e^- \rightarrow dye \quad (16)$$

To obtain a higher efficiency in converting absorbed light into direct electrical energy (for solar cells) or hydrogen energy, fast electron injection and slow backward reaction are required. Based on the literature on electron/hole recombination of dyes, the recombination times were found to be mostly in the order of nanoseconds to microseconds, sometimes in milliseconds, while the electron injection times were in the order of femtoseconds. The fast electron injection and slow backward reaction make dye-sensitized semiconductors feasible for energy conversion.

Gurunathan *et al.* (1997) investigated the effects of different dyes on photocatalytic hydrogen production by SnO_2 with and without a sacrificial agent,

such as EDTA. The band gap of SnO_2 is 3.5 eV and, hence, it could not be excited by visible light. After SnO_2 was sensitized by dyes, hydrogen production was observed under visible light illumination. Qualitatively, the ranking of dyes in terms of the degree of enhancement of hydrogen production rate was found in the following order: Eosin Blue > Rose Bengal > $Ru(bpy)_3^{2+}$ > Rhodamine B ~ Acriflavin > Fluorescein. However, based on the structures and properties of these dyes, a general conclusion could not be drawn. For example, Rhodamine B showed the longest absorption wavelength maxima together with more negative reduction potential (-0.545 V) than CB level (-0.34 V) of SnO_2, but it did not increase hydrogen production rate significantly. Therefore, the difference in their electron injection characteristics may be the reason for the variation in hydrogen production rates. However, comparison of electron injection characteristics among these dyes was not available. Further research work is thus required to compare dynamics of charge excitation, recombination, and electron injection of different dyes to gain a better understanding of the mechanisms behind the phenomena.

Eosin-sensitized TiO_2 under visible light irradiation was investigated by Jin *et al.* (2006). For the sensitizer suspension system, the electrons excited by visible light were injected into the conduction band (CB) of TiO_2, at which the CB acted as a mediator for transferring electrons from the sensitizer to substrate of electrons acceptors on TiO_2 surface. It was observed that Eosin Y preferred to adsorb on metal atom rather than on TiO_2 of surface. Eosin Y-sensitized N-doped TiO_2 was also studied (Li *et al.*, 2008). The results showed that Eosin Y makes TiO_2 and N-TiO_2 have a very strong adsorption in region of visible light.

2.10 Composite Semiconductors

Semiconductor composite (coupling) is another method to utilize visible light for hydrogen production. When a large band gap semiconductor is coupled with a small band gap semiconductor with a more negative CB level, CB electrons can be injected from the small band gap semiconductor to the large band gap semiconductor. Thus, a wide electron-hole separation is achieved, as shown in Figure 2.14. The process is similar to dye sensitization. The difference is that electrons are injected

from one semiconductor to another semiconductor, rather than from excited dye to semiconductor. Successful coupling of the two semiconductors for photocatalytic hydrogen production under visible light irradiation can be achieved when the following conditions are met: (1) semiconductors should be photocorrosion free, (2) the small band gap semiconductor should be able to be excited by visible light, (3) the CB of the small band gap semiconductor should be more negative than that of the large band gap semiconductor, (4) the CB of the large band gap semiconductor should be more negative than the reduction potential of H^+/H_2, and (5) electron injection should be fast, as well as efficient.

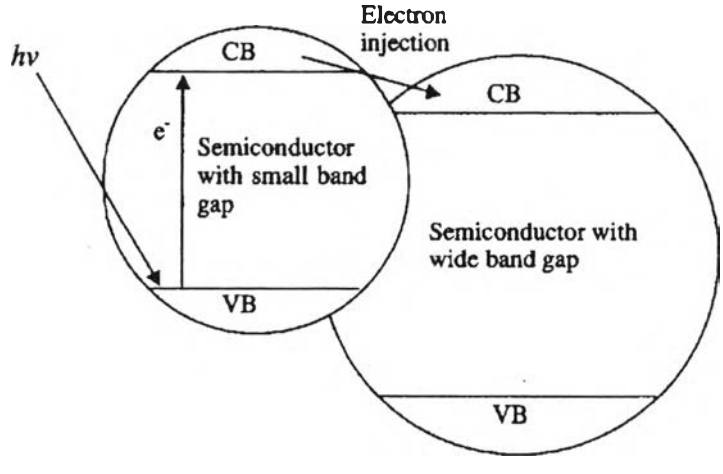

Figure 2.14 Electron injection in composite semiconductors.

It has been reported that coupling of CdS (band gap of 2.4 eV) with SnO_2 (band gap of 3.5 eV) could produce hydrogen under visible radiation (Gurunathan *et al.*, 1997). Electrons excited to the CB (-0.76 eV) of CdS are injected to the CB (-0.34 eV) of SnO_2 in less than 20 ps, resulting in wide electron-hole separation. Sacrificial agent, EDTA, has to be added to scavenge VB hole on CdS; otherwise, photocorrosion of CdS would occur. Doong *et al.* (2001) coupled CdS with TiO_2 for 2-chlorophenol degradation under UV irradiation. In the study, both CdS and TiO_2 could be excited.

The combination of the two semiconductors showed better photocatalytic activity due to better charge separation. The CB electrons of CdS are injected to the

CB of TiO_2, while the VB holes in TiO_2 are injected to the VB of CdS. Kang *et al.* (1999) employed CdS-TiO_2 composite semiconductor for 4-chlorophenol photodegradation and found that coupling of CdS with TiO_2 was more effective than CdS and TiO_2 used separately. The composite semiconductor CdS-TiO_2 can be applied to produce hydrogen since the CB of TiO_2 is more negative than hydrogen production level. So *et al.* (2004) conducted photocatalytic hydrogen production using CdS-TiO_2 composite semiconductors. Photocorrosion of CdS was prevented by addition of Na_2S. Optical absorption spectra analysis showed that CdS-TiO_2 composite semiconductors could absorb photons with wavelength up to 520 nm. Under visible light illumination (Xe lamp), CdS-TiO_2 composite semiconductors produced hydrogen at a higher rate than CdS and TiO_2 used separately.

Recently, Li *et al.* (2004) developed a novel photocatalyst by a combination of nitrogen doping and composite semiconductors. N-doped ZnO was coupled with WO_3, V_2O_5, and Fe_2O_3 for acetaldehyde decomposition under visible light irradiation. By doping with nitrogen, ZnO could respond with visible spectrum. Unlike coupling with WO_3 and V_2O_5, coupling with Fe_2O_3 caused the photocatalytic activity to deteriorate since Fe_2O_3 served as both an electron sink and a hole sink. Although N-doped ZnO-WO_3 and ZnO-V_2O_5 worked better under visible light irradiation for acetaldehyde decomposition, they were not suitable for hydrogen production since the CB of both WO_3 and V_2O_5 are not negative enough. It is expected that a N-doped composite semiconductor with CB level more negative than hydrogen production level, such as SiC-TiO_2, may serve as an efficient photocatalyst for hydrogen production under visible light irradiation.

2.11 Mixed Oxide System

The investigation of a mixed oxide system is very promising topic since such a system can be used as a base for new composite materials. The characteristics of such materials can be regulated and controlled in advance through changes in their composition. Investigations have proved good prospects for designing materials containing a photoactive semiconductor (TiO_2) and an admixture (SiO_2, ZrO_2, ZnO, Al_2O_3, Bi_2O_3, HfO_2, V_2O_5, WO_3, etc.) with different chemical compositions. The

latter substances are also widely used as pigments and catalysts, components of photolayers, and dielectric materials. They can also be used as promising source materials for ceramics. The same materials can be used for solar energy transformation and accumulation, toxic industrial waste treatment, in information recording systems, and in new industrial lines of low-tonnage synthesis of important products (Kobasa and Kondratyeva, 2008)

Particularly, TiO_2-SiO_2 mixed oxide represents a novel class of materials that have attracted much attention in recent years. The applications of TiO_2-SiO_2 materials as catalysts and supports fall into three categories based on their unique physico-chemical properties: (i) photocatalyst that is associated with the support effect and the quantum-size effect; (ii) acid catalyst that is related to the generation of new acid sites; and (iii) excellent catalytic support materials that possess enhanced thermal and mechanical stability due to SiO_2 while preserving the catalytic performance of TiO_2. The understanding of the structural characteristics of TiO_2-SiO_2 and the relationships with the physicochemical/reactivity properties is also of great importance in a wide range of applied sciences. Therefore, the TiO_2-SiO_2 mixed and supported oxides as catalysts, excluding Ti-silicalites, have been investigated and developed with special emphasis on the structural characterization and establishment of the relationships between the structural characteristics and the physicochemical/reactivity properties (Gao and Wachs, 1999).

Schattka *et al.* (2002) investigated the photocatalytic activities of porous TiO_2 and TiO_2-ZrO_2 structures prepared by a polymer gel templating technique. The results showed that the mixed TiO_2-ZrO_2 network structures exhibited higher surface areas than pure TiO_2 network, as well as an increased surface area and a decrease of the anatase to rutile crystal phase transformation. The combination of binary metal oxides is interesting in order to improve catalytic performance, such as excellent transport behavior, large porosity, and specific surface area.

The preparation of TiO_2-SiO_2 and TiO_2-ZrO_2 mixed oxides by a sol–gel method was studied (Jung and Park, 2004). It was reported that the surface area of TiO_2-SiO_2 mixed oxide was proportionally increased with increasing SiO_2 content; besides, TiO_2-SiO_2 and TiO_2-ZrO_2 mixed oxides had photocatalytic activity in linear relationship with the crystallite size of anatase phase. That is, larger crystallite size

led to higher photoactivity of TiO_2-SiO_2 and TiO_2-ZrO_2 mixed oxides. Also, the thermal stability of TiO_2 for the phase transition from anatase to rutile was greatly improved and made it possible to calcine the prepared mixed oxides at higher temperature without any formation of rutile phase.

Furthermore, pure titania and zirconia have been extensively studied as catalyst support for heterogeneous catalytic reactions which prepare by the sol–gel method (Zou and Lin, 2004). The result showed that pure titania and pure zirconia had lower surface area than the mixed oxides calcined at the same calcination temperatures. It was also found that doping ZrO_2 retarded the phase transformation from anatase to rutile.

Rungjaroentawon (2011) studied the hydrogen production from photocatalytic water splitting under visible light irradiation using Eosin Y-sensitized mesoporous-assembled TiO_2-SiO_2 mixed oxide photocatalysts loaded with monometallic and bimetallic Pt-Au cocatalysts, of which the mesoporous-assembled TiO_2-SiO_2 mixed oxide photocatalyst with various TiO_2-to-SiO_2 molar ratios were synthesized by a sol-gel process. The results showed that without metal loading, the TiO_2-SiO_2 photocatalyst with a TiO_2-to-SiO_2 molar ratio of 97:3 calcined at 500 °C provided the maximum photocatalytic hydrogen production activity.

Besides, over Ag loaded mesoporous assembled TiO_2-ZrO_2 mixed oxide nanocrystal photocatalysts can improve hydrogen production activity (Onsuratoom *et al.*, 2011). The TiO_2-ZrO_2 mixed oxides with various TiO_2-to-ZrO_2 molar ratios were synthesized by a sol-gel process. The results showed that the TiO_2-ZrO_2 mixed oxide nanocrystal photocatalyst with a TiO_2-to-ZrO_2 molar ratio of 93:7 calcined at 500 °C exhibited the highest photocatalytic hydrogen production activity, and the Ag loading of 0.5 wt.%.

Moreover, the photocatalytic activity of the mesoporous-assembled $SrTi_xZr_{1-x}O_3$ nanocrystal photocatalysts for degradation of Acid Black (AB) diazo dye used by varying Ti-to-Zr was studied by Khunrattanaphon et al. (2011). The experimental results exhibited that without Pt loading, the mesoporous-assembled $SrTi_xZr_{1-x}O_3$ photocatalyst with a Ti-to-Zr molar fraction of 0.9:0.1 (i.e.$SrTi_{0.9}Zr_{0.1}O_3$) calcined at 700 °C for 4 h provided a maximum degradation rate constant as compared to the other $SrTi_xZr_{1-x}O_3$ photocatalysts. The optimum Pt

loading of 1 wt.% by a single-step sol–gel method on the mesoporous-assembled $SrTi_{0.9}Zr_{0.1}O_3$photocatalyst was found to greatly increase the degradation rate constant of the AB dye.

2.12 Bimetallic System

Bimetallic catalysts have attracted extensive attention because of their markedly different properties from either of the constituent metals, and have often enhanced catalytic stabilities, activities, and/or selectivities (Li *et al.*, 2007). And, bimetallic nanoparticles are particularly important in the field of catalysis because the interactions between the two components in bimetallic nanoparticles introduce a mutual influence on the neighboring atoms, which leads to unique electronic and structural properties of the nanoparticles and improves catalytic activity of monometallic nanoparticles.

A bimetallic catalyst have been found to be more active than a monometallic catalyst and had lower apparent activation energy. Normally, Pt is used in photocatalytic reaction. Moreover, the addition of Au to result in the formation of Pt-Au bimetallic catalyst is more activite than other bimetallic catalysts. In particular, supported bimetallic Pt–Au nanoparticles are of fundamental interest and importance. Furthermore, Au is one of only two transition metals more electronegative than Pt, so the incorporation of Au into Pt nanoparticles may have unique effects on catalysis/photocatalysis by Pt (Betany *et al.*, 2007).

The photocatalytic activities of monometallic Au and bimetallic Ag/Au modified-titania were studied (Zielińska-jurek *et al.*, 2011). The results exhibited that the Au/Ag-TiO_2 has higher photoactivity than Ag-TiO_2 and Au-TiO_2 photocatalysts. The mechanism of photocatalytic oxidation of phenol is shown in Figure 2.15. The increase in photocatalytic activity after modification of titania with bimetallic Ag/Au is due to participation of additional metal in a mechanism of electron transfer. The mechanism of this reaction is as follows: (1) the photons are absorbed by Ag/Au particles, (2) the electrons is transferred from excited noble metal nanoparticle to conduction band of tiatania and consecutively to adsorbed oxygen, and (3) phenol molecule is oxidized by O_2^- with the formation of benzoquinone on the surface of

Ag/Au. The low photocatalytic activities of composites with monometallic loading substantiated the necessity of electronic contact between Au and Ag nanoparticles.

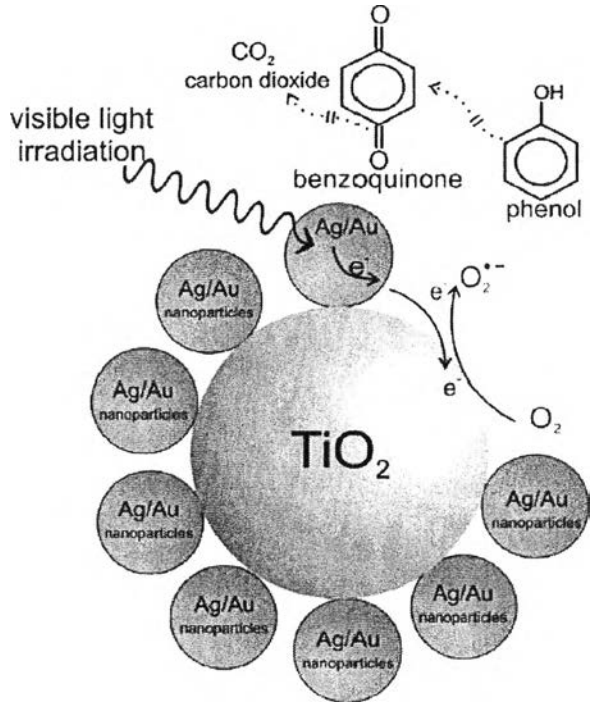

Figure 2.15 Proposed mechanism of phenol degradation at the surface of Ag/Au-TiO_2 nanoparticles (Zielińska-jurek *et al.*, 2011).

2.13 Porous Material

The classification of pores according to size has been under discussion for many years, but in the past, the terms ''micropore'' and ''macropore'' have been applied in different ways by physical chemists and some other scientists. With an attempt to clarify this situation, the limits of size of the different categories of pores included in Table 2.1 have been proposed by the International Union of Pure and Applied Chemistry (IUPAC) (Ishizaki *et al.*, 1988; Rouquerol *et al.*, 1999). As indicated, the ''pore size'' is generally specified as the ''pore width'', i.e. the available distance between the two opposite walls. Obviously, pore size has a precise meaning when the geometrical shape is well defined. Nevertheless, for most

purposes, the limiting size is that of the smallest dimension, and this is generally taken to represent the effective pore size.

Table 2.1 Definitions about porous solids

Term	Definition
Porous solid	Solid with cavities or channels which are deeper than they are wide
Micropore	Pore of internal width less than 2 nm
Mesopore	Pore of internal width between 2 and 50 nm
Macropore	Pore of internal width greater than 50 nm
Pore size	Pore width (diameter of cylindrical pore or distance between opposite walls of slit)
Pore volume	Volume of pores determined by stated method
Surface area	Extent of total surface area determined by given method under stated conditions

According to the IUPAC classification, porous materials are regularly organized into three categories on a basis of predominant pore size as follows:

- Microporous materials (pore size < 2 nm) include amorphous silica and inorganic gel to crystalline materials, such as zeolites, aluminophosphates, gallophosphates, and related materials.
- Mesoporous materials (2 nm ≤ pore size ≤ 50 nm) include the M41S family (e.g. MCM-41, MCM-48, MCM-50, etc.) and other non-silica materials synthesized via intercalation of layered materials, such as double hydroxides, metal (titanium, zirconium) phosphates, and clays.
- Macroporous materials (pore size > 50 nm) include glass-related materials, aerogels, and xerogels.

Nowadays, micro- and mesoporous materials are generally called ''nanoporous materials''. Particularly, mesoporous materials are remarkably very

suitable for catalysis applications, whereas the pores of microporous materials may become easily plugged during catalyst preparation if high metal loading is required.

2.14 Sol-Gel Process

The sol-gel process has been intensively studied because it is so effective to prepare nano-sized mesoporous materials (Sreethawong *et al.*, 2005). Because the metal oxides are also deactivated due to sintering or crystal growth during their continuous use in high temperature processes, and the catalytic performance of the metal oxides is well-known to depend on their specific surface area, sol–gel method presents some particular advantages through a low-temperature process, avoiding contamination of the materials. It also yields better stoichiometric control and the possibility of grain-size and grain-shape control. This technique does not require complicated instruments, such as in chemical vapor deposition method. It provides a simple and easy means of synthesizing nano-sized particles, which is essential for nano-catalysts (Wu *et al.*, 2004). It involves the formation of metal-oxo-polymer network from molecular precursors, such as metal alkoxides, and subsequent polycondensation as follows:

$$\text{M-OR} + \text{H}_2\text{O} \rightarrow \text{M-OH} + \text{ROH} \quad (17)$$

$$\text{M-OH} + \text{M-OR} \rightarrow \text{M-O-M} + \text{R-OH} \quad (18)$$

$$\text{M-OH} + \text{M-OH} \rightarrow \text{M-O-M} + \text{H}_2\text{O} \quad (19)$$

where M = Ti, Si, Zr, Al, etc., and R = alkyl group.

All stages, including the formation of colloid particles to form gel network, drying of wet gel, and calcination stage, can all lead to grain growth and formation of agglomerates. Hence, to carefully control the process is very essential in preparing high-performance and high-reliability powders. The relative rates of hydrolysis and polycondensation strongly influence the structure and properties of the resulting metal oxides. Typically, sol-gel-derived precipitates are amorphous in nature, requiring further heat treatment to induce crystallization. The calcination process frequently gives rise to particle agglomeration and grain growth and may induce phase transformation (Wang *et al.*, 1999). Thus, a surfactant is used to prevent agglomeration of the particle. The $BaTiO_3$ nanoparticles synthesized by sol-gel

process (Yu *et al.*, 2008), however, are easy to form agglomeration. This can be avoided by the application of the surfactant, i.e. oleic acid as cheap and innoxious surfactant, thus preventing the agglomeration of particles. The sol–gel process by the addition of surfactant can help to enforce size controllability and prepare well-dispersed powders. The ideal model of forming the $BaTiO_3$ is shown in Figure 2.16.

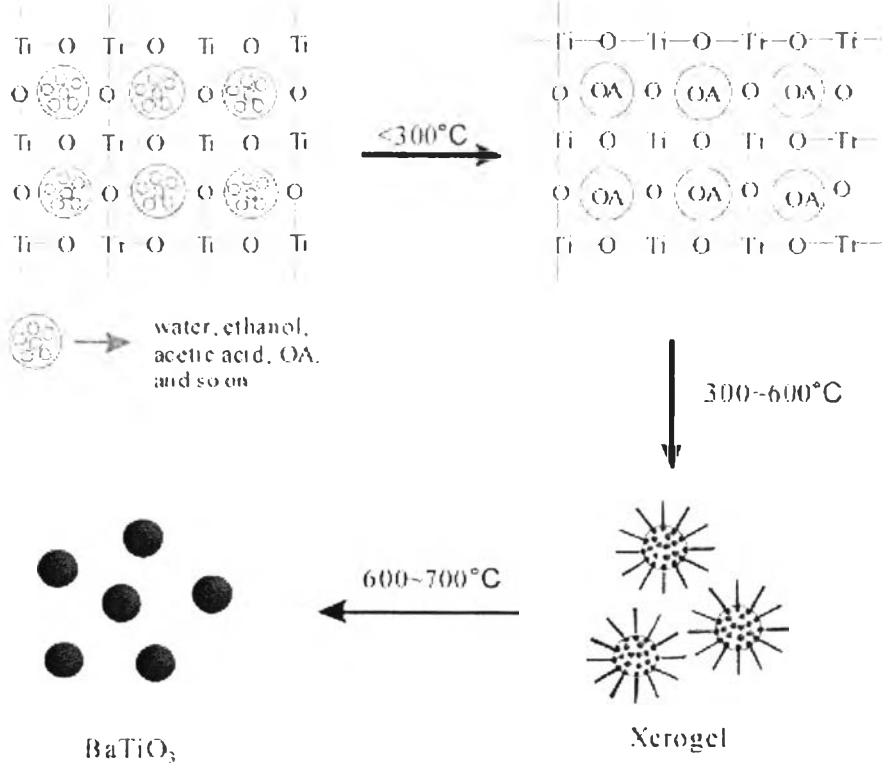

Figure 2.16 A schematic of forming the $BaTiO_3$ nanoparticles (Yu *et al.*, 2008).

The process can be divided to three steps. Firstly, oleic acid (OA) enchases in the 3D network structure of -Ti-O-Ti- when the temperature is lower than 300°C. Secondly, between 300 and 600°C, a number of "microcapsules" of $BaTiO_3$ precursors coated by OA are formed. The carboxyl of OA is towards the inside and hydrophobic -R group towards the outside. Excessive OA as solution will allow the system to form "micro-capsules". Finally, when the temperature is higher than 600°C, OA decomposes, and the walls of "microcapsules" are destroyed. Although this happens, the shape of $BaTiO_3$ precursor is preserved, thus producing better-dispersed $BaTiO_3$ nanoparticles.

The mesoporous-assembled $SrTiO_3$ nanocrystal photocatalyst could also be synthesized by a sol-gel process with the aid of structure-directing surfactant and used for photodegradation of methy orange (Puangpetch *et al.*, 2008). The different solvents resulted in different gel formation characteristics and different amounts of water required for gel formation. The use of ethanol (EtOH) as the solvent yielded a $SrTiO_3$ photocatalysts with a higher purity than that synthesized using ethylene glycol (EG) or the EtOH/EG mixture. The pore size distribution was found to be very narrow and monomodal when LAHC was used as a structure-directing surfactant. The mesoporous-assembled structure with a high pore uniformity of $SrTiO_3$ plays the most important role affecting the photocatalytic activity of the $SrTiO_3$ photocatalyst. The $SrTiO_3$ with the mesoporous-assembled structure and narrow pore size distribution synthesized at a calcination temperature of 700°C, a heating rate of 1°C/min, a LAHC-to-TIPT molar ratio of 0.25:1, and using an EtOH solvent provided the highest photocatalytic degradation activity, which was much higher than that of the non-mesoporous-structured commercial $SrTiO_3$.